

Noise representation in residuals of LSQR, LSMR, and CRAIG regularization

Iveta Hnětynková*

Marie Kubínová†

Martin Plešinger‡

Abstract

Golub-Kahan iterative bidiagonalization represents the core algorithm in several regularization methods for solving large linear noise-polluted ill-posed problems. We consider a general noise setting and derive explicit relations between (noise contaminated) bidiagonalization vectors and the residuals of bidiagonalization-based regularization methods LSQR, LSMR, and CRAIG. For LSQR and LSMR residuals we prove that the coefficients of the linear combination of the computed bidiagonalization vectors reflect the amount of propagated noise in each of these vectors. For CRAIG the residual is only a multiple of a particular bidiagonalization vector. We show how its size indicates the regularization effect in each iteration by expressing the CRAIG solution as the exact solution to a modified compatible problem. Validity of the results for larger two-dimensional problems and influence of the loss of orthogonality is also discussed.

Keywords ill-posed problems, regularization, Golub-Kahan iterative bidiagonalization, LSQR, LSMR, CRAIG

AMS classification 15A29, 65F10, 65F22

1 Introduction

In this paper we consider ill-posed linear algebraic problems of the form

$$b = Ax + \eta, \quad A \in \mathbb{R}^{m \times n}, \quad b \in \mathbb{R}^m, \quad \|\eta\| \ll \|Ax\|, \quad (1)$$

where the matrix A represents a discretized smoothing operator with the singular values decaying gradually to zero without a noticeable gap. We assume that multiplication of a vector v by A or A^T results in smoothing which reduces the relative size of the high-frequency components of v . The operator A and the vector b are supposed to be known. The vector η represents errors, such as *noise*, that affect the exact data. Problems of this kind are commonly referred to as linear discrete ill-posed problems or linear inverse problems and arise in a variety of applications [1, 2]. Since A is ill-conditioned, the presence of noise makes the naive solution

$$x^{\text{naive}} \equiv A^\dagger b,$$

where A^\dagger denotes the Moore-Penrose pseudoinverse, meaningless. Therefore, to find an acceptable numerical approximation to x , it is necessary to use regularization methods.

*Faculty of Mathematics and Physics, Charles University, Prague, Czech Republic. Electronic address: hnetynko@karlin.mff.cuni.cz

†Faculty of Mathematics and Physics, Charles University, Prague, Czech Republic, and Institute of Computer Science, The Czech Academy of Sciences, Prague, Czech Republic. Electronic address: kubinova@karlin.mff.cuni.cz ✉

‡Faculty of Education, Technical University of Liberec, Liberec, Czech Republic. Electronic address: martin.plesinger@tul.cz

Various techniques to regularize the linear inverse problem (1) have been developed. For large-scale problems, iterative regularization is a good alternative to direct regularization methods. When an iterative method is used, regularization is achieved by early termination of the process, before noise η starts to dominate the approximate solution [1]. Many iterative regularization methods such as LSQR [3, 4, 5, 6], CRAIG [7, 8], LSMR [9], and CRAIG-MR/MRNE [10, 11] involve the Golub-Kahan iterative bidiagonalization [12]. Combination with an additional inner regularization (typically with a spectral filtering method) gives so-called hybrid regularization; see, for example, [4, 13, 14, 15]. Various approaches for choosing the stopping criterion, playing here the role of the regularization parameter, are based on comparing the properties of the actual residual to an a priori known property of noise, such as the noise level in the Morozov's discrepancy principle [16], or the noise distribution in the cumulative residual periodogram method [17, 18, 19]. Thus understanding how noise translates to the residuals during the iterative process is of great interest.

The aim of this paper is, using the analysis of the propagation of noise in the left bidiagonalization vectors provided in [20], to study the relation between residuals of bidiagonalization-based methods and the noise vector η . Whereas in [20], white noise was assumed, here we have no particular assumptions on the distribution of noise. We only assume the amount of noise is large enough to make the noise propagation visible through the smoothing by A in construction of the bidiagonalization vectors. This is often the case in ill-posed problems, as we illustrate on one-dimensional (1D) as well as significantly noise contaminated two-dimensional (2D) benchmarks. We prove that LSQR and LSMR residuals are given by a linear combination of the bidiagonalization vectors with the coefficients related to the amount of propagated noise in the corresponding vector. For CRAIG, the residual is only a multiple of a particular bidiagonalization vector. This allows us to prove that an approximate solution obtained in a given iteration by CRAIG applied to (1) coincides with an exact solution of the (compatible) modified problem

$$Ax = b - \tilde{\eta}, \quad (2)$$

where $\tilde{\eta}$ is a noise vector estimate constructed from the currently computed bidiagonalization vectors. These results contribute to understanding of regularization properties of the considered methods and should be considered when devising reliable stopping criteria.

Note that since LSQR is mathematically equivalent to CGLS and CGNR, CRAIG is mathematically equivalent to CGNE and CGME [21], and LSMR is mathematically equivalent to CRLS [9], then in exact arithmetic, the analysis applies also to these methods.

The paper is organized as follows. In Section 2, after a recollection of the previous results, we study the propagation of various types of noise and the influence of the loss of orthogonality on this phenomenon. Section 3 investigates the residuals of selected methods with respect to the noise contamination in the left bidiagonalization vectors and compares their properties. Section 4 discusses validity of obtained results for larger 2D problems. Section 5 concludes the paper.

Unless specified otherwise, we assume exact arithmetic and the presented experiments are performed with full double reorthogonalization in the bidiagonalization process. Throughout the paper, $\|v\|$ denotes the standard Euclidean norm of the vector v , vector e_k denotes the k -th column of the identity matrix. By \mathcal{P}_k , we denote the set of polynomials of degree less or equal to k . The noise level is denoted by $\delta_{\text{noise}} \equiv \|\eta\|/\|Ax\|$. By Poisson noise, we understand $b_i \sim \text{Pois}([Ax]_i)$, i.e., the right-hand side b is a Poisson random with the Poisson parameter Ax . The test problems were adopted from the Regularization tools [22]. For simplicity of exposition, we assume the initial approximation $x_0 \equiv 0$ throughout the paper. Generalization to $x_0 \neq 0$ is straightforward.

2 Properties of the Golub-Kahan iterative bidiagonalization

2.1 Basic relations

Given the initial vectors $w_0 \equiv 0$, $s_1 \equiv b/\beta_1$, where $\beta_1 \equiv \|b\|$, the Golub-Kahan iterative bidiagonalization [12] computes, for $k = 1, 2, \dots$,

$$\begin{aligned}\alpha_k w_k &= A^T s_k - \beta_k w_{k-1}, & \|w_k\| &= 1, \\ \beta_{k+1} s_{k+1} &= A w_k - \alpha_k s_k, & \|s_{k+1}\| &= 1,\end{aligned}\tag{3}$$

until $\alpha_k = 0$ or $\beta_{k+1} = 0$, or until $k = \min(m, n)$. Vectors s_1, \dots, s_k , and w_1, \dots, w_k , form orthonormal bases of the Krylov subspaces $\mathcal{K}_k(AA^T, b)$ and $\mathcal{K}_k(A^T A, A^T b)$, respectively. In the rest of the paper, we assume that the bidiagonalization process does not terminate before the iteration $k + 1$, i.e., $\alpha_l, \beta_{l+1} > 0$, $l = 1, \dots, k$.

Denoting $S_k \equiv [s_1, \dots, s_k] \in \mathbb{R}^{m \times k}$, $W_k \equiv [w_1, \dots, w_k] \in \mathbb{R}^{n \times k}$ and

$$L_k \equiv \begin{bmatrix} \alpha_1 & & & \\ \beta_2 & \alpha_2 & & \\ & \ddots & \ddots & \\ & & \beta_k & \alpha_k \end{bmatrix} \in \mathbb{R}^{k \times k}, \quad L_{k+} \equiv \begin{bmatrix} L_k \\ e_k^T \beta_{k+1} \end{bmatrix} \in \mathbb{R}^{(k+1) \times k},$$

we can write the matrix version of the bidiagonalization as

$$A^T S_k = W_k L_k^T, \quad A W_k = S_{k+1} L_{k+}.$$

The two corresponding Lanczos three-term recurrences

$$(AA^T)S_k = S_{k+1}(L_{k+}L_k^T), \quad (A^T A)W_k = W_{k+1}(L_{k+1}^T L_{k+}),$$

allow us to describe the bidiagonalization vectors s_{k+1} and w_{k+1} in terms of the Lanczos polynomials as

$$s_{k+1} = \varphi_k(AA^T)b, \quad w_{k+1} = \psi_k(A^T A)A^T b \quad \varphi_k, \psi_k \in \mathcal{P}_k;\tag{4}$$

see [3, 4, 23, 24, 25]. From (4) we have that

$$s_{k+1} = \varphi_k(AA^T)b = \varphi_k(AA^T)(Ax + \eta),$$

giving

$$s_{k+1} = [\varphi_k(AA^T)Ax + (\varphi_k(AA^T) - \varphi_k(0))\eta] + \varphi_k(0)\eta.\tag{5}$$

The first component on the right-hand side of (5) can be rewritten as

$$s_{k+1}^{\text{LF}} \equiv [\varphi_k(AA^T)Ax + (\varphi_k(AA^T) - \varphi_k(0))\eta] = Aq_{k-1}(AA^T)[x + A^T \eta],$$

for some $q_{k-1} \in \mathcal{P}_k$. Since A has the smoothing property, then s_{k+1}^{LF} is smooth for $k \ll \min(m, n)$. Thus s_{k+1} is a sum of a low-frequency vector and the scaled noise vector η ,

$$s_{k+1} = s_{k+1}^{\text{LF}} + \varphi_k(0)\eta.\tag{6}$$

Note that this splitting corresponds to the low-frequency part and propagated (non-smoothed) noise part only when $\|s_{k+1}^{\text{LF}}\|^2 + \|\varphi_k(0)\eta\|^2 \approx 1$. For large ks , there is a considerable cancellation between s_{k+1}^{LF} and $\varphi_k(0)\eta$, the splitting (6) still holds but it does not correspond to our intuition of an underlying smooth vector and some added scaled noise. Thus we restrict ourselves to smaller values of k .

It has been shown in [20] that whereas for s_1 (the scaled right-hand side) the noise part in (6) is small compared to the true data, for larger k , due to the smoothing property of the matrix A and the orthogonality

between the vectors s_k , the noise part becomes more significant. The noise scaling factor determining the relative amplification of the non-smoothed part of noise corresponds to the constant term of the Lanczos polynomial

$$\varphi_k(0) = (-1)^k \frac{1}{\beta_{k+1}} \prod_{j=1}^k \frac{\alpha_j}{\beta_j} \quad (7)$$

called the *amplification factor*.¹ Its behavior for problems with white noise was studied in [20] and the analysis concludes that its size increases with k until the *noise revealing iteration* k_{rev} , where the vector s_{k+1} is dominated by the non-smoothed part of noise. Then the amplification factor increases at least for one iteration. The noise revealing iteration k_{rev} can be defined as Note that there is no analogy for the right bidiagonalization vectors, since all vectors w_k are smoothed and the factor $\psi_k(0)$ on average grows till late iterations. A recursive relation for $\psi_k(0)$, obtained directly from (3) has the form

$$\begin{aligned} \psi_0(0) &= \frac{1}{\alpha_1 \beta_1}, \\ \psi_k(0) &= \frac{1}{\alpha_{k+1}} (\varphi_k(0) - \beta_{k+1} \psi_{k-1}(0)), \quad k = 1, 2, \dots \end{aligned} \quad (8)$$

2.2 Behavior of the noise amplification factor

Influence of the noise frequency characteristics The phenomenon of noise amplification is demonstrated on the problems from [26, 22]. Figures 1b and 1c show the absolute terms of the Lanczos polynomials φ_k and ψ_k for the problem **shaw** polluted with white noise of various noise levels. For example, for the noise level 10^{-3} , the maximum of $\varphi_k(0)$ is achieved for $k = 6$, which corresponds to the observation that the vector s_7 in Figure 1a is the most dominated by propagated noise. Obviously, the noise revealing iteration increases with decreasing noise level. The amplification factors exhibit similar behavior before the first decrease. However, the behavior of $\varphi_k(0)$ can be more complicated. In Figure 2a for **phillips**, the sizes of the amplification factors oscillate as a consequence of the oscillations in the sizes of the spectral components of b in the left singular subspaces of A . Thus there is a partial reduction of the noise component, which influences the subsequent iterations, even before the noise revealing iteration.

Even though [20] assumed white noise, noise amplification can be observed also for other noise settings and the formulas (4)-(8) still hold. However, for high-frequency noise, there is smaller cancellation between the low-frequency component s_{k+1}^{LF} and the noise part $\varphi_k(0)\eta$ in (6). Therefore, in the orthogonalization steps succeeding the noise revealing iteration k_{rev} , the noise part is projected out more significantly. For low-frequency noise, on the other side, this smoothing is less significant, which results in smaller drop of (7) after k_{rev} . This is illustrated in Figure 2b on the problem **shaw** polluted by red (low-frequency), white, and violet (high-frequency) noise of the same noise level. For spectral characteristics of these types of noise see Figure 3. Figure 2c shows the amplification factor for various levels of Poisson noise.

Influence of the loss of orthogonality First note that the splitting (6) remains valid even if φ_k are not exactly orthonormal Lanczos polynomials, since the propagated noise can be still tracked using the absolute term of the corresponding (computed) polynomial. Nevertheless, it is clear that the loss of orthogonality among the left bidiagonalization vectors in finite precision arithmetic influences the behavior of the amplification factor φ_k , i.e. the propagation of noise. In the following, we denote all quantities computed without reorthogonalization by hat. Loss of orthogonality can be detected, e.g., by tracking the size of the smallest singular value $\bar{\sigma}_{\min}$ of the matrix \hat{S}_k of the computed left bidiagonalization vectors. In Figure 4 (left) for the problem **shaw** and **gravity** we see that when $\bar{\sigma}_{\min}$ drops below one detecting the loss of orthogonality among its columns, the size of the amplification factor $\hat{\varphi}_k(0)$ starts to oscillate. However, except of the delay, the larger values of $|\hat{\varphi}_k(0)|$ still match those of $|\varphi_k(0)|$. If we plot $|\hat{\varphi}_k(0)|$ against the rank of \hat{S}_k instead of k , the

¹Note that in [20] a different notation was used. The Lanczos polynomial φ_k was scaled by $\|b\|$ so that $s_{k+1} = \bar{\varphi}_k(AA^T)s_1$. The vector s_{k+1} was split into $s_{k+1} = s_{k+1}^{\text{exact}} + s_{k+1}^{\text{noise}}$. In our notation, $s_{k+1}^{\text{exact}} = s_{k+1}^{\text{LF}}$, and $s_{k+1}^{\text{noise}} = \varphi_k(0)\eta$.

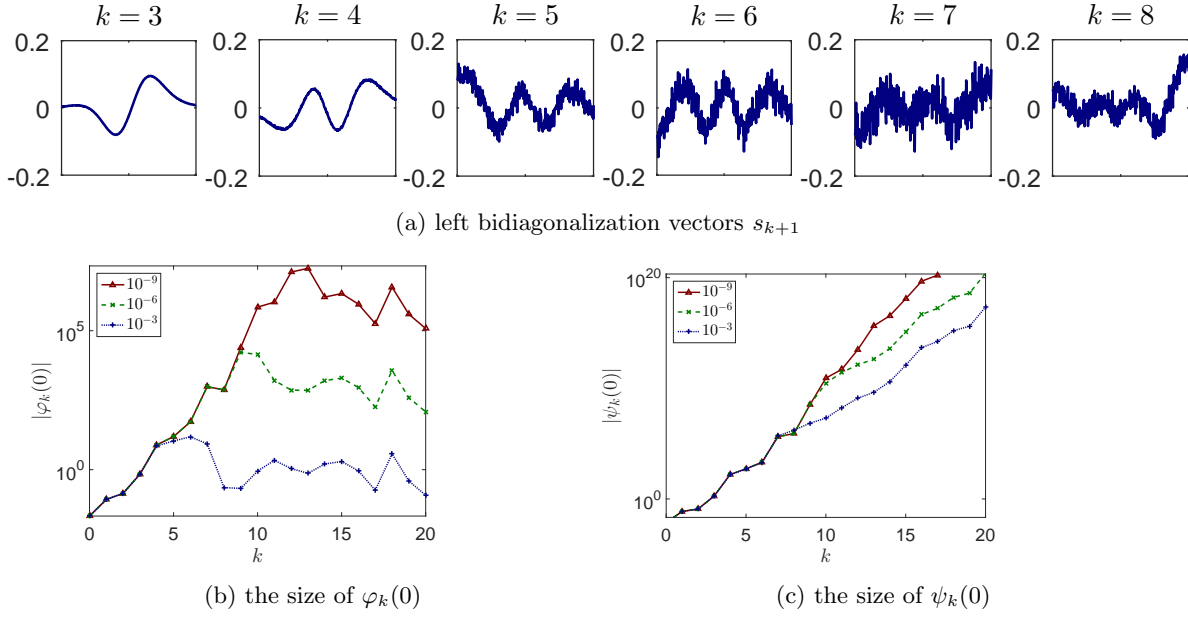


Figure 1: The problem **shaw**(400) polluted by white noise: (a) the left bidiagonalization vectors s_{k+1} for the noise level 10^{-3} ; (b) the size of the absolute term of the Lanczos polynomial φ_k for various noise levels; (c) the size of the absolute term of the Lanczos polynomial ψ_k for various noise levels.

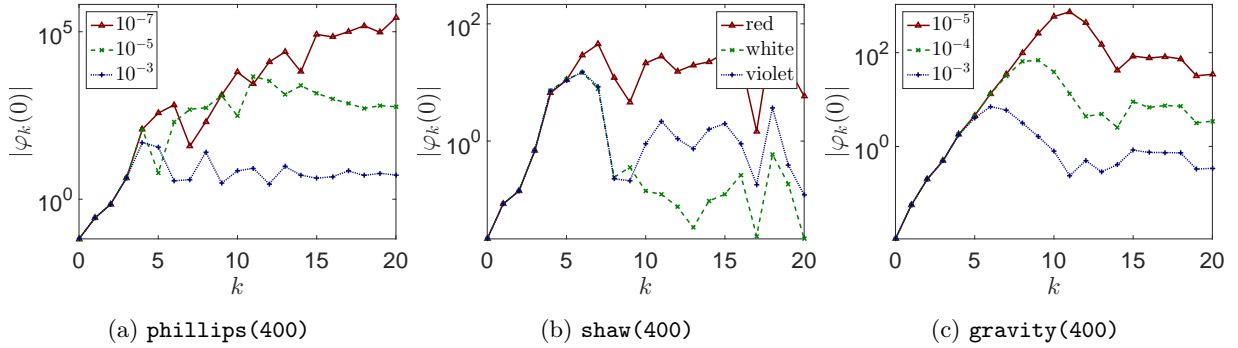


Figure 2: Influence of the amount of noise and its frequency characteristics on the amplification factor (7): (a) the problem **phillips** with various noise levels of white noise; (b) the problem **shaw** with noise of different frequency characteristics; (c) the problem **gravity** with Poisson noise with different noise levels achieved by scaling.

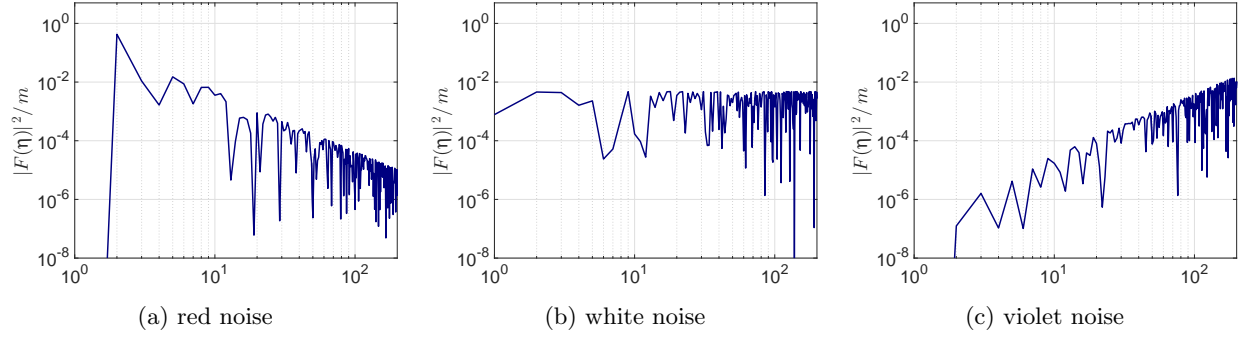


Figure 3: Power spectral densities (or simply power spectra) for red (low-frequency dominated), white (or Gaussian), and violet (high-frequency dominated) noise η , $\|\eta\| = 1$. Power spectrum is given by squared magnitudes of Fourier coefficients $F(\eta)$ of η (see, e.g., [27, chap. 2.7]), here computed by the discrete Fourier transform. Power spectra are normalized by the length of the vector.

sizes of the two amplification factors become very similar. In our experiments, the rank of \hat{S}_k was computed as `rank(S(:,1:k),1e-1)` in MATLAB, i.e., singular values of \hat{S}_k at least ten times smaller than they would be for orthonormal columns were considered zero. A similar shifting strategy was proposed in [28, chap. 3] for the convergence curves of the conjugate gradient method. Note that the choice of the tolerance can be problem dependent. Further study of this phenomenon is beyond the scope of this paper, but we can conclude that except of the delay the noise revealing phenomenon is in finite precision computations present.

3 Noise in the residuals of iterative methods

CRAIG [7], LSQR [3], and LSMR [9] represent three methods based on the Golub-Kahan iterative bidiagonalization. At the k -th step, they search for the approximation of the solution in the subspace generated by vectors w_1, \dots, w_k , i.e.,

$$x_k = W_k y_k, \quad y_k \in \mathbb{R}^k. \quad (9)$$

The corresponding residual has the form

$$r_k \equiv b - Ax_k = b - AW_k y_k = S_{k+1}(\beta_1 e_1 - L_{k+1} y_k). \quad (10)$$

CRAIG minimizes the distance of x_k from the naive solution yielding

$$L_k y_k^{\text{CRAIG}} = \beta_1 e_1. \quad (11)$$

LSQR minimizes the norm of the residual r_k yielding

$$y_k^{\text{LSQR}} = \underset{y \in \mathbb{R}^k}{\operatorname{argmin}} \|\beta_1 e_1 - L_{k+1} y\|. \quad (12)$$

LSMR minimizes the norm of $A^T r_k$ giving

$$y_k^{\text{LSMR}} = \underset{y \in \mathbb{R}^k}{\operatorname{argmin}} \|\beta_1 \alpha_1 e_1 - L_{k+1}^T L_{k+1} y\|. \quad (13)$$

These methods are mathematically equivalent to Krylov subspace methods based on the Lanczos tridiagonalization (particularly Lanczos for linear systems and MINRES) applied to particular normal equations. The relations useful in the following derivations are summarized in Table 1.

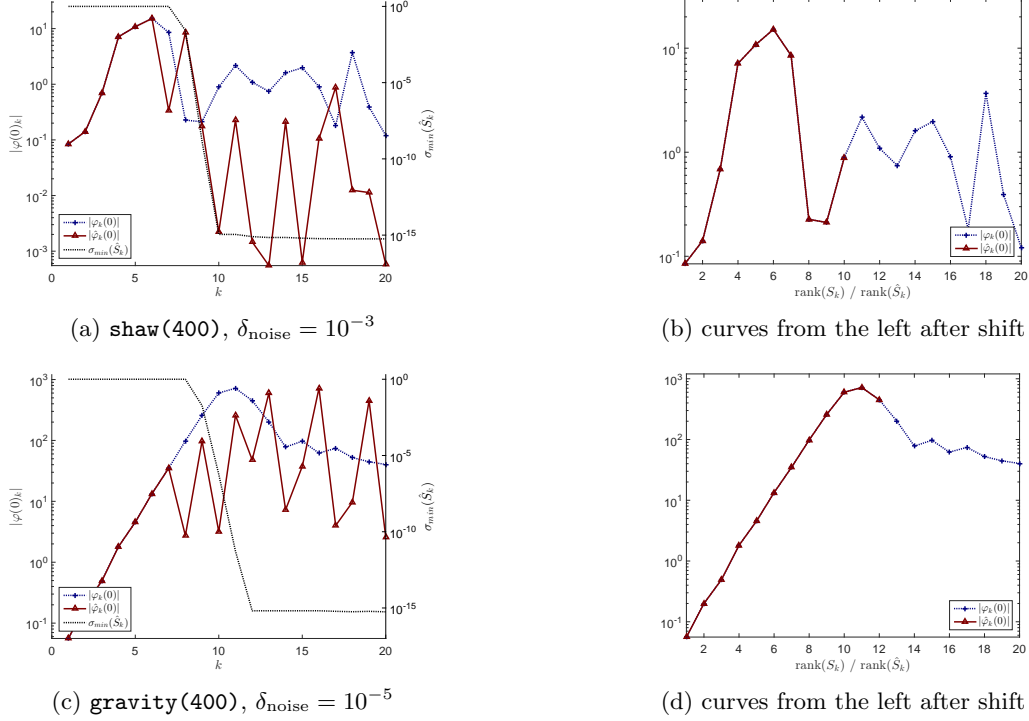


Figure 4: Illustration of the noise amplification for the problem **shaw** and **gravity** in finite precision computations. Left: The sizes of the amplification factor (7) computed with full double reorthogonalization ($\varphi_k(0)$) and without reorthogonalization ($\hat{\varphi}_k(0)$). Right: $|\hat{\varphi}_k(0)|$ plotted against $\text{rank}(\hat{S}_k)$ computed as `rank(S(:,1:k),1e-1)` in MATLAB, together with $|\varphi_k(0)|$ plotted against $\text{rank}(S_k) = k$.

Table 1: Interpretation of bidiagonalization-based methods (CRAIG, LSQR, LSMR) as tridiagonalization-based methods (Lanczos for linear systems, MINRES) applied to the corresponding normal equations. In last two columns, the solution x of the bidiagonalization-based methods is obtained from their tridiagonalization counterparts as $x = A^T y$ and $x = A^T A z$, respectively. See also [9].

method/equation	$(A^T A)x = A^T b$	$(A A^T)y = b$	$(A^T A)z = A^\dagger b$
Lanczos method	LSQR(A, b)	CRAIG(A, b)	—
MINRES	LSMR(A, b)	LSQR(A, b)	CRAIG(A, b)

Since Lanczos method is a Galerkin (residual orthogonalization) method, we immediately see that

$$\begin{aligned} r_k^{\text{CRAIG}} &= (-1)^k \|r_k^{\text{CRAIG}}\| s_{k+1}, \\ A^T r_k^{\text{LSQR}} &= (-1)^k \|A^T r_k^{\text{LSQR}}\| w_{k+1}. \end{aligned} \quad (14)$$

Using the relation between the Galerkin and the residual minimization method, see [21, sec. 6.5.7], we obtain,

$$\begin{aligned} \|r_k^{\text{LSQR}}\| &= \frac{1}{\sqrt{\sum_{l=0}^k 1/\|r_l^{\text{CRAIG}}\|^2}}, \\ \|A^T r_k^{\text{LSMR}}\| &= \frac{1}{\sqrt{\sum_{l=0}^k 1/\|A^T r_l^{\text{LSQR}}\|^2}}. \end{aligned} \quad (15)$$

Note that these equations hold, up to a small perturbation, also in finite precision computations. See [29] for more details.

In the rest of this section, we investigate the residuals of each particular method. We focus on in which sense the residuals approximate the noise vector. We discuss particularly the case when noise contaminates the bidiagonalization vectors fast and thus the noise revealing iteration is well defined. More general discussion follows in Section 4.

3.1 CRAIG residuals

The following result relates approximate solution obtained by CRAIG for (1) to the solution of the problem with the same matrix and a modified right-hand side.

Proposition 1. *Consider the first k steps of the Golub-Kahan iterative bidiagonalization. Then the approximation x_k^{CRAIG} defined in (9) and (11), is an exact solution to a consistent problem*

$$Ax = b - \varphi_k(0)^{-1} s_{k+1}. \quad (16)$$

Consequently,

$$\|r_k^{\text{CRAIG}}\| = |\varphi_k(0)|^{-1}. \quad (17)$$

Proof. First note that we only need to show that $r_k^{\text{CRAIG}} = \varphi_k(0)^{-1} s_{k+1}$, $k = 1, 2, \dots$. From (14) and (4) it follows that there exist $c \in \mathbb{R}$, such that

$$r_k^{\text{CRAIG}} = c \cdot s_{k+1} = c \cdot \varphi_k(AA^T)b.$$

Let us now determine the constant c . From (10) and (4), we have that

$$r_k^{\text{CRAIG}} = \Pi_k(AA^T)b, \quad \text{where } \Pi_k \in \mathcal{P}_k \text{ and } \Pi_k(0) = 1.$$

Combining these two equations, we obtain

$$r_k^{\text{CRAIG}} = \varphi_k(0)^{-1} \varphi_k(AA^T)b. \quad (18)$$

Substituting to (18) back from (4), we immediately have (16). Since $\|s_{k+1}\| = 1$, (17) is a direct consequence of (16). \square \square

Although the relation (16) is valid for any problem of the form (1), it has a particularly interesting interpretation for inverse problems with a smoothing operator A . Suppose we neglect the low-frequency part s_{k+1}^{LF} in (6) and estimate the unknown noise η from the left bidiagonalization vector s_{k+1} as

$$\eta \approx \tilde{\eta} \equiv \varphi_k(0)^{-1} s_{k+1}. \quad (19)$$

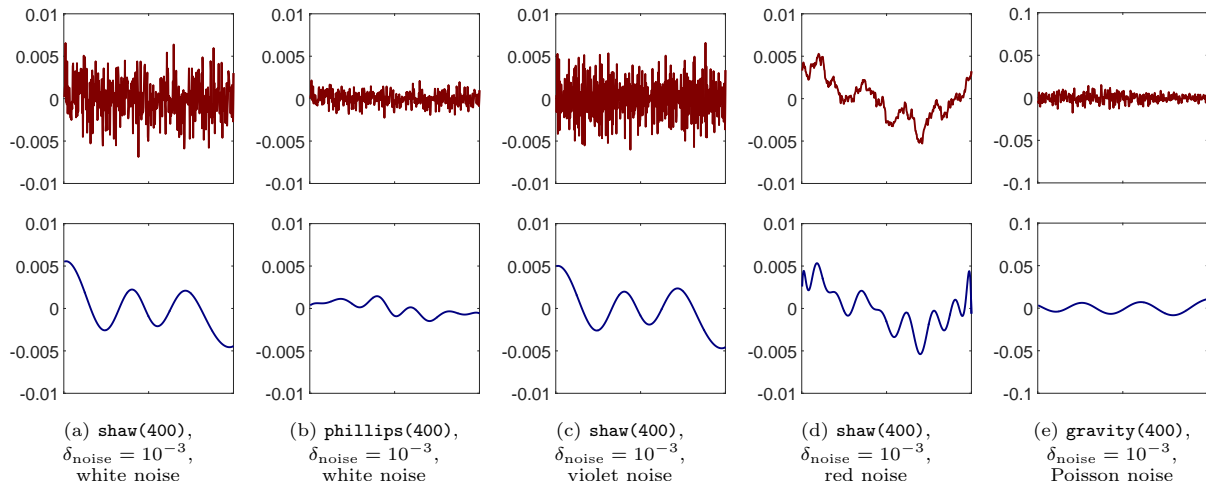


Figure 5: Illustration of the quality of the noise vector approximation $\tilde{\eta}$ obtained by (19) for $k = k_{\text{rev}} + 1$ on various test problems and various characteristics of noise. Upper: The original noise vector η . Lower: The difference $\eta - \tilde{\eta}$.

Subtracting $\tilde{\eta}$ from b in (1), we obtain exactly the modified problem (16). Thus Proposition 1 in fact states that in each iteration k , x_k^{CRAIG} represents the exact solution of the problem (2) with noise being approximated by a particular re-scaled left bidiagonalization vector.

The norm of the CRAIG residual r_k^{CRAIG} is inversely proportional to the amount of noise propagated to the currently computed left bidiagonalization vector. It reaches its minimum exactly in the noise revealing iteration $k = k_{\text{rev}}$, which corresponds to the iteration with (19) being the best approximation of the unknown noise vector. The actual noise vector η and the difference $\eta - \tilde{\eta}$ for $\tilde{\eta}$ obtained from $s_{k_{\text{rev}}+1}$ are compared in Figure 5; see also [30]. We see that in iteration k_{rev} , the troublesome high-frequency part of noise is perfectly removed. The remaining perturbation only contains smoothed, i.e., low-frequency part of the original noise vector. The match in (17) remains valid, up to a small perturbation, also in finite precision computations, since the noise propagation is preserved, see Section 2.2

Note that due to different frequency characteristic of η and s_{k+1}^{LF} for small k , there is a relatively small cancellation between them and

$$\|s_{k+1}^{\text{LF}}\|^2 + \|\varphi_k(0)\eta\|^2 \approx 1.$$

This gives

$$\|(b - \tilde{\eta}) - Ax\| = \|\varphi_k(0)^{-1}s_{k+1}^{\text{LF}}\| \approx |\varphi_k(0)|^{-1}\sqrt{1 - \|\varphi_k(0)\eta\|^2} = \sqrt{|\varphi_k(0)|^{-2} - \|\eta\|^2}$$

supporting our expectation that the size of the remaining perturbation depends on how closely the inverse amplification factor $|\varphi_k(0)|^{-1}$ approaches $\|\eta\|$.

We may also conclude that for ill-posed problems with a smoothing operator A , the minimal error $\|x_k^{\text{CRAIG}} - x\|$ is reached approximately at the iteration with the maximal noise revealing, i.e., with the minimal residual. This is confirmed by numerical experiments in Figure 6 comparing $\|x_k^{\text{CRAIG}} - x\|$ with $\|r_k^{\text{CRAIG}}\|$ for various test problems and noise characteristics, both with and without reorthogonalization.

3.2 LSQR residuals

Whereas for CRAIG, the residual is just a scaled left bidiagonalization vector, for LSQR it is a linear combination of all previously computed left bidiagonalization vectors. Indeed,

$$r_k^{\text{LSQR}} = b - AW_k y_k^{\text{LSQR}} = S_{k+1} \left(\beta_1 e_1 - L_{k+1} y_k^{\text{LSQR}} \right), \quad (20)$$

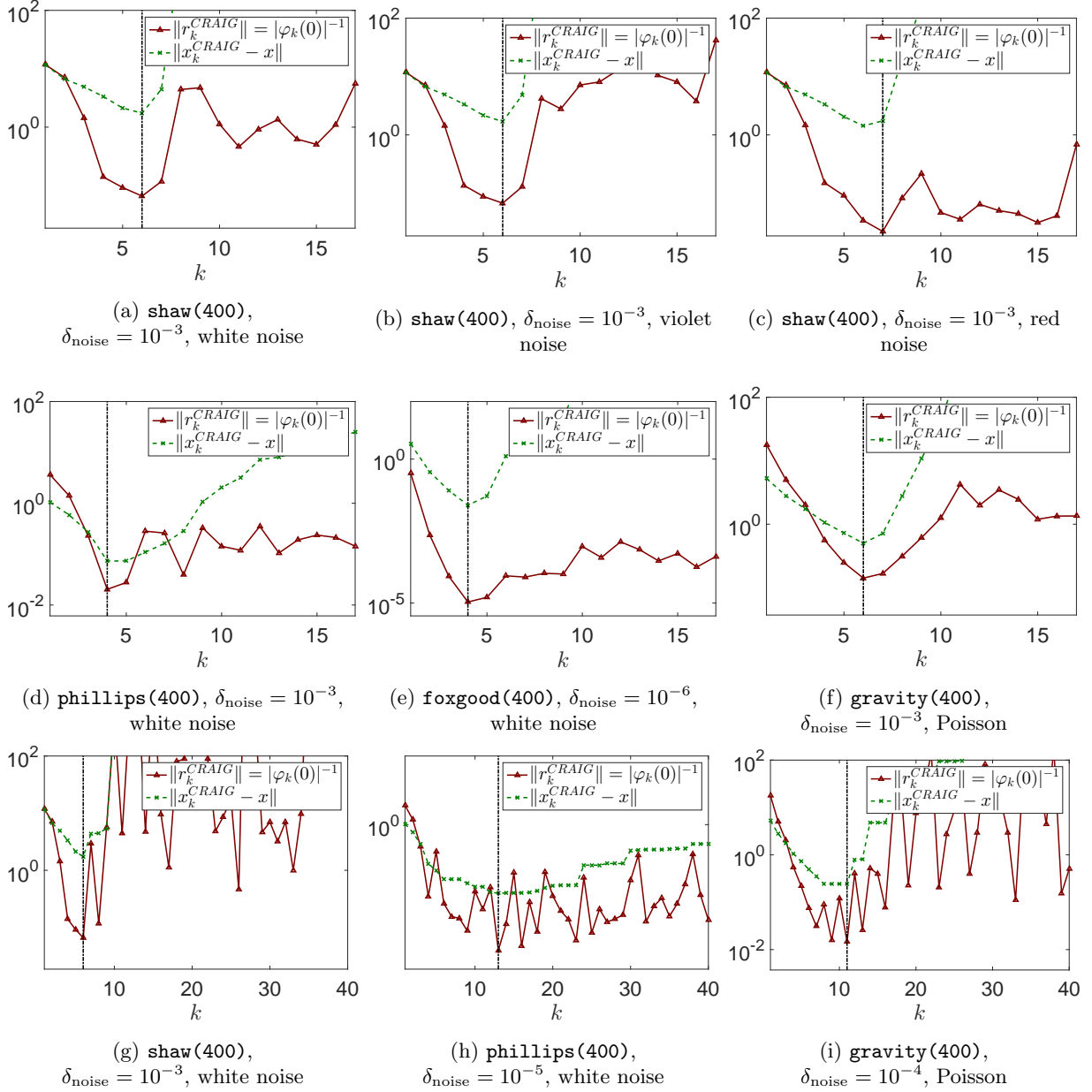


Figure 6: Comparison of the size of the residual and the size of the error in CRAIG for various test problems with various noise characteristics. The minimal error is achieved approximately when the residual is minimized (vertical line). In Figures (g)-(i) without reorthogonalization.

see (10). The entries of the residual of the projected problem

$$p_k^{\text{LSQR}} \equiv \beta_1 e_1 - L_{k+} y_k^{\text{LSQR}}, \quad (21)$$

see (12), represent the coefficients of the linear combination in (20). The following proposition shows the relation between the coefficients and the amplification factor $\varphi_k(0)$.

Proposition 2. *Consider the first k steps of the Golub-Kahan iterative bidiagonalization. Let $r_k^{\text{LSQR}} = b - Ax_k^{\text{LSQR}}$, where x_k^{LSQR} is the approximation defined in (9) and (12). Then*

$$r_k^{\text{LSQR}} = \frac{1}{\sum_{l=0}^k \varphi_l(0)^2} \sum_{l=0}^k \varphi_l(0) s_{l+1}. \quad (22)$$

Consequently,

$$\|r_k^{\text{LSQR}}\| = \frac{1}{\sqrt{\sum_{l=0}^k \varphi_l(0)^2}}.$$

Proof. Since

$$y_k^{\text{LSQR}} = \underset{y}{\operatorname{argmin}} \|\beta_1 e_1 - L_{k+} y\|,$$

we get

$$L_{k+}^T p_k^{\text{LSQR}} = 0.$$

It follows from the structure of the matrix L_{k+} that the entries of p_k^{LSQR} satisfy

$$\alpha_l e_l^T p_k^{\text{LSQR}} + \beta_{l+1} e_{l+1}^T p_k^{\text{LSQR}} = 0, \quad \text{for } l = 1, \dots, k.$$

Thus

$$p_k^{\text{LSQR}} = c_k \begin{bmatrix} \varphi_0(0) \\ \varphi_1(0) \\ \vdots \\ \varphi_k(0) \end{bmatrix}, \quad (23)$$

where c_k is a factor that changes with k . From (15) and (18) it follows that

$$\|p_k^{\text{LSQR}}\| = \|r_k^{\text{LSQR}}\| = \frac{1}{\sqrt{\sum_{l=0}^k \varphi_l(0)^2}}. \quad (24)$$

By comparing (23) and (24), we get

$$c_k = \frac{1}{\sum_{l=0}^k \varphi_l(0)^2},$$

which together with (20) and (21) yields (22). □ □

In other words, Proposition 2 says that the coefficients of the linear combination (20) follow the behavior of the amplification factor in the sense that representation of a particular left bidiagonalization vector s_{l+1} in the residual r_k^{LSQR} , $k \geq l$, is proportional to the amount of propagated non-smoothed part of noise η in this vector.

Relation (22) also suggests that the norm-minimizing process (LSQR) and the corresponding Galerkin process (CRAIG) provide similar solutions whenever

$$\frac{\varphi_k(0)^2}{\sum_{l=0}^k \varphi_l(0)^2} \approx 1,$$

i.e., whenever the noise revealing in the last left bidiagonalization vector s_{k+1} is much more significant than in all previous left bidiagonalization vectors s_1, \dots, s_k , i.e., typically before we reach the noise revealing iteration. This is confirmed numerically in Figure 7, comparing the semiconvergence curves of CRAIG and LSQR.

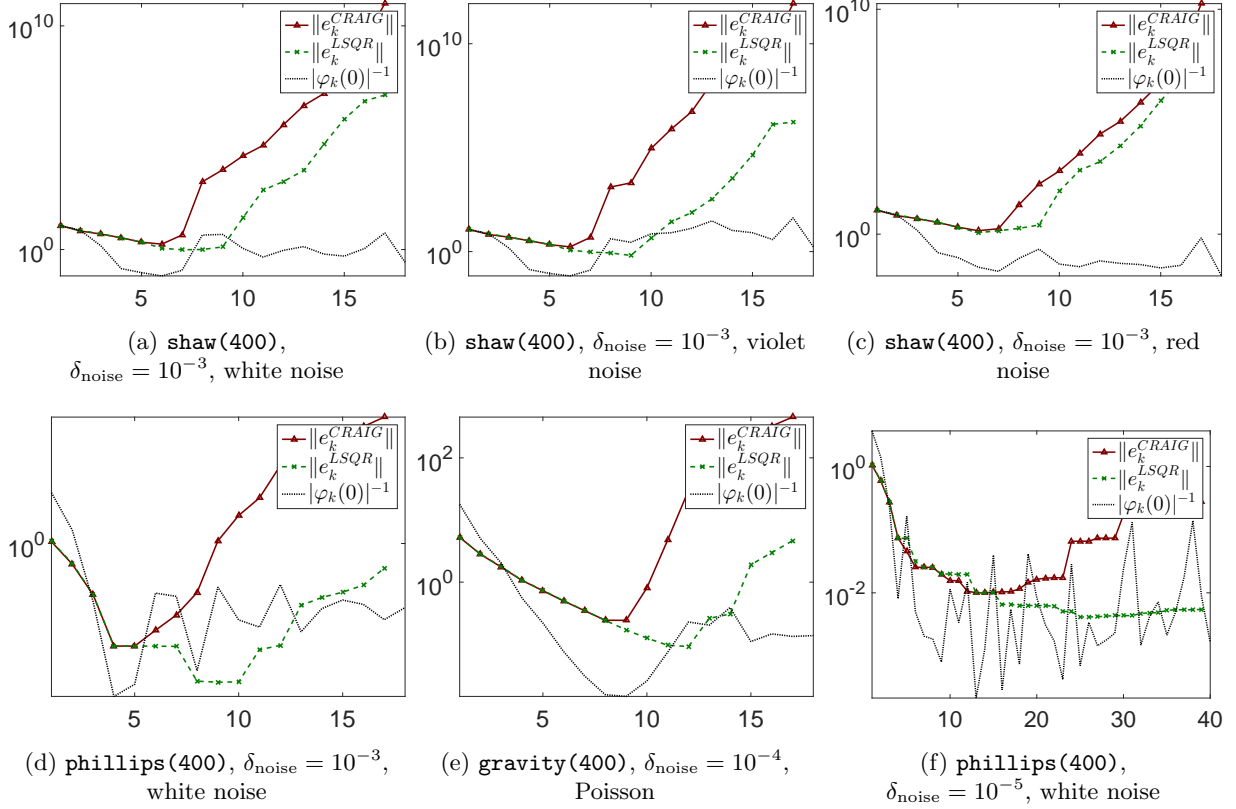


Figure 7: The size of the error of LSQR and CRAIG in comparison with the inverse of the amplification factor for various test problems with various noise characteristics. The semiconvergence curves exhibit similar behavior until the noise revealing iteration. In Figure (f) without reorthogonalization.

3.3 LSMR residuals

Before we investigate the residual of LSMR with respect to the basis S_k , we should understand how it is related to the residual of LSQR. It follows from Table 1 that the relation between $A^T r_k^{\text{LSMR}}$ and $A^T r_k^{\text{LSQR}}$ is analogous to the relation between r_k^{CRAIG} and r_k^{LSQR} . Using Proposition 1 and 2, with φ_k substituted by ψ_k and s_k substituted by w_k , we obtain

$$A^T r_k^{\text{LSQR}} = \psi_k(0)^{-1} w_{k+1},$$

and

$$A^T r_k^{\text{LSMR}} = \frac{1}{\sum_{l=0}^k \psi_l(0)^2} \sum_{l=0}^k \psi_l(0) w_{l+1}.$$

Since

$$A^T r_k^{\text{LSMR}} = W_{k+1} L_{k+1}^T p_k^{\text{LSMR}},$$

we obtain that

$$L_{k+1}^T p_k^{\text{LSMR}} = \frac{1}{\sum_{l=0}^k \psi_l(0)^2} \begin{bmatrix} \psi_0(0) \\ \psi_1(0) \\ \vdots \\ \psi_k(0) \end{bmatrix}. \quad (25)$$

This equality however does not provide the desired relationship between the residuals r_k^{LSMR} themselves and the left bidiagonalization vectors s_1, \dots, s_{k+1} . This is given in the following proposition.

Proposition 3. *Consider the first k steps of the Golub-Kahan iterative bidiagonalization. Let $r_k^{\text{LSMR}} = b - Ax_k^{\text{LSMR}}$, where x_k^{LSMR} is the approximation defined in (9) and (13). Then*

$$r_k^{\text{LSMR}} = \frac{1}{\sum_{l=0}^k \psi_l(0)^2} \sum_{l=0}^k \left(\varphi_l(0) \sum_{j=l}^k \alpha_{j+1}^{-1} \varphi_j(0)^{-1} \psi_j(0) \right) s_{l+1}.$$

Proof. From (25) it follows that

$$p_k^{\text{LSMR}} = \frac{1}{\sum_{l=0}^k \psi_l(0)^2} L_{k+1}^{-T} \begin{bmatrix} \psi_0(0) \\ \psi_1(0) \\ \vdots \\ \psi_k(0) \end{bmatrix},$$

where L_{k+1}^{-T} is an upper triangular matrix with entries

$$e_i^T L_{k+1}^{-T} e_j = \begin{cases} \frac{1}{\alpha_j} & (\text{if } i = j) \\ (-1)^{i-j} \frac{\beta_{i+1} \cdots \beta_j}{\alpha_i \cdots \alpha_j} & (\text{if } i < j) \end{cases} = \frac{\varphi_{i-1}(0)}{\alpha_j \varphi_{j-1}(0)}.$$

Thus

$$p_k^{\text{LSMR}} = \frac{1}{\sum_{l=0}^k \psi_l(0)^2} \text{triu} \left(\begin{bmatrix} \varphi_0(0) \\ \varphi_1(0) \\ \vdots \\ \varphi_k(0) \end{bmatrix} \begin{bmatrix} \varphi_0(0)^{-1} \\ \varphi_1(0)^{-1} \\ \vdots \\ \varphi_k(0)^{-1} \end{bmatrix}^T \right) \begin{bmatrix} \alpha_1^{-1} \psi_0(0) \\ \alpha_2^{-1} \psi_1(0) \\ \vdots \\ \alpha_{k+1}^{-1} \psi_k(0) \end{bmatrix},$$

where $\text{triu}(\cdot)$ extracts the upper triangular part of the matrix. Multiplying out, we obtain

$$p_k^{\text{LSMR}} = \frac{1}{\sum_{l=0}^k \psi_l(0)^2} \begin{bmatrix} \varphi_0(0) \sum_{l=0}^k \alpha_{l+1}^{-1} \varphi_l(0)^{-1} \psi_l(0) \\ \varphi_1(0) \sum_{l=1}^k \alpha_{l+1}^{-1} \varphi_l(0)^{-1} \psi_l(0) \\ \vdots \\ \varphi_{k-1}(0) \sum_{l=k-1}^k \alpha_{l+1}^{-1} \varphi_l(0)^{-1} \psi_l(0) \\ \varphi_k(0) \alpha_{k+1}^{-1} \varphi_k(0)^{-1} \psi_k(0) \end{bmatrix}.$$

□

□

Here the sizes of coefficients in p_k^{LSMR} need careful discussion. From (7) and (8) it follows that the absolute terms of the Lanczos polynomials $\varphi_l(0)$ and $\psi_l(0)$ have the same sign. Thus we have

$$\alpha_{l+1}^{-1} \varphi_l(0)^{-1} \psi_l(0) > 0, \quad \forall l = 0, 1, \dots$$

and therefore the sum

$$\sum_{l=j}^k \alpha_{l+1}^{-1} \varphi_l(0)^{-1} \psi_l(0) \quad (26)$$

decreases when j increases. Furthermore, it was shown in [20, sec. 3.2] that for $j < k_{\text{rev}}$

$$\alpha_l \approx \beta_l.$$

Thus (7) yields

$$\sum_{l=j}^k \alpha_{l+1}^{-1} \varphi_l(0)^{-1} \psi_l(0) \approx \sum_{l=j}^k \psi_l(0).$$

However, since $|\varphi_j(0)|$ on average increases rapidly with j (see Section 2.2), the sizes of the entries of p_k^{LSMR} in (3.3) generally increase with l before k_{rev} . After j reaches the noise revealing iteration k_{rev} , $|\varphi_j(0)|$ decreases at least for one but typically for more subsequent iterations; see Section 2.2. Multiplication by the decreasing (26) causes that the size of the entries in (3.3) can be expected to decrease after k_{rev} .

From the previous we conclude that the behavior of the entries of p_k^{LSMR} resembles the behavior of $\varphi_l(0)$, i.e., the size of a particular entry is proportional to the amount of propagated noise in the corresponding bidiagonalization vector, similarly as in the LSQR method. Figure 8 compares the entries of p_k^{LSMR} with appropriately re-scaled amplification factor $\varphi_k(0)$ on the problem **shaw** with white noise. We see that the difference is negligible and therefore the residuals for LSQR and LSMR resemble. In early iterations, the resemblance of the residuals indicates resemblance of the solutions since the remaining perturbation only contains low frequencies, which are not amplified by A^\dagger .

Note also that since $\psi_k(0)$ grows rapidly on average, see Figure 1c in Section 2.2, we may expect

$$\frac{\psi_k(0)^2}{\sum_{l=0}^k \psi_l(0)^2} \approx 1.$$

Therefore $A^T r_k^{\text{LSMR}}$ resembles $A^T r_k^{\text{LSQR}}$ giving another explanation why LSMR and LSQR behave similarly for inverse problems with a smoothing operator A , see Figure 9 for a comparison on several test problems.

Figure 10 illustrates the match between the noise vector and residual of CRAIG, LSQR and LSMR method. We see that while CRAIG residual resembles noise only in the noise revealing iteration, LSQR and LSMR are less sensitive to the particular number of iterations k as the residuals are combinations of bidiagonalization vectors with appropriate coefficients. Moreover, the best match in LSQR and LSMR method overcomes the best match in CRAIG. This is caused by the fact that the remaining low-frequency part is efficiently suppressed by the linear combination.

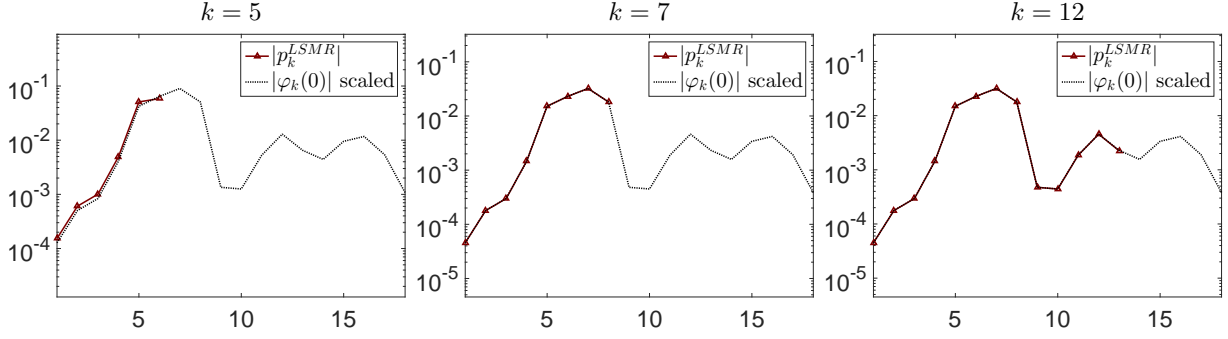


Figure 8: The componets of p_k^{LSQR} vs. the size of the amplification factor $\varphi_k(0)$ (after scaling) for several values of k for the problem **shaw** with white noise, $\delta_{\text{noise}} = 10^{-3}$. The differences are negligible.

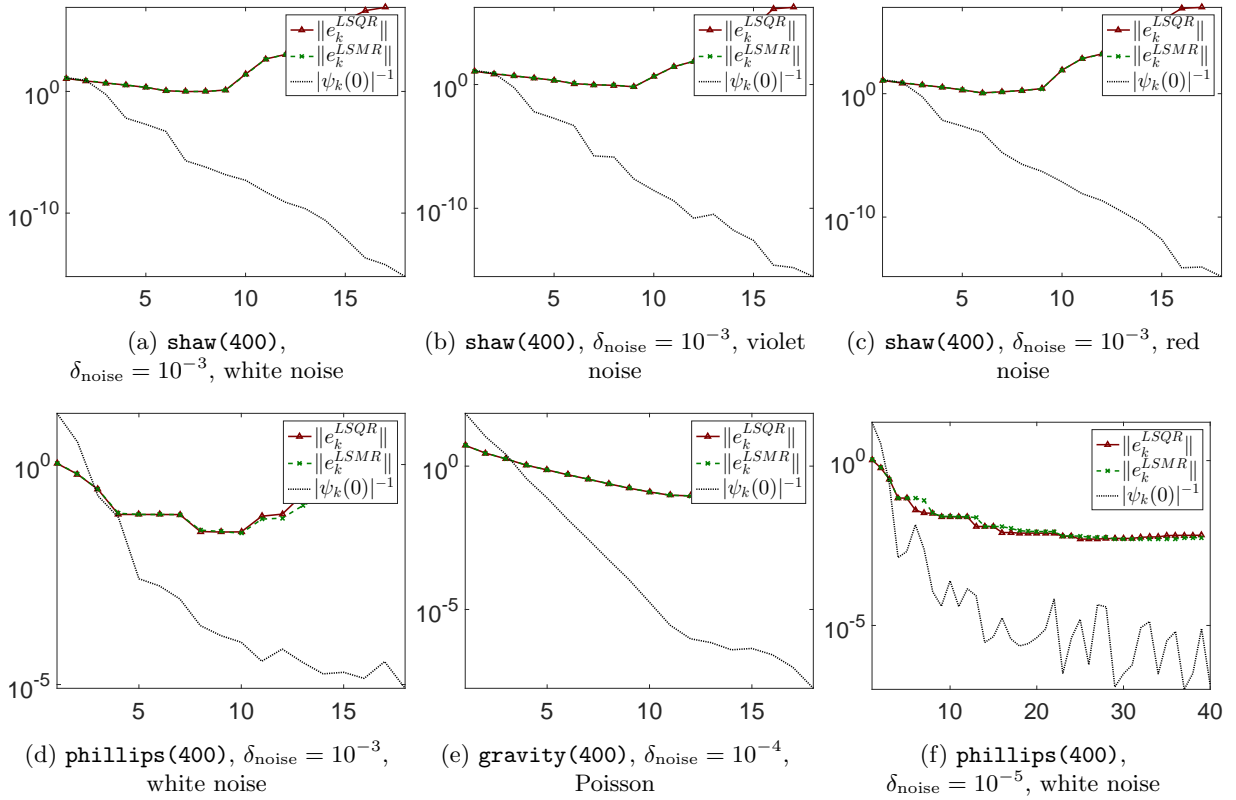
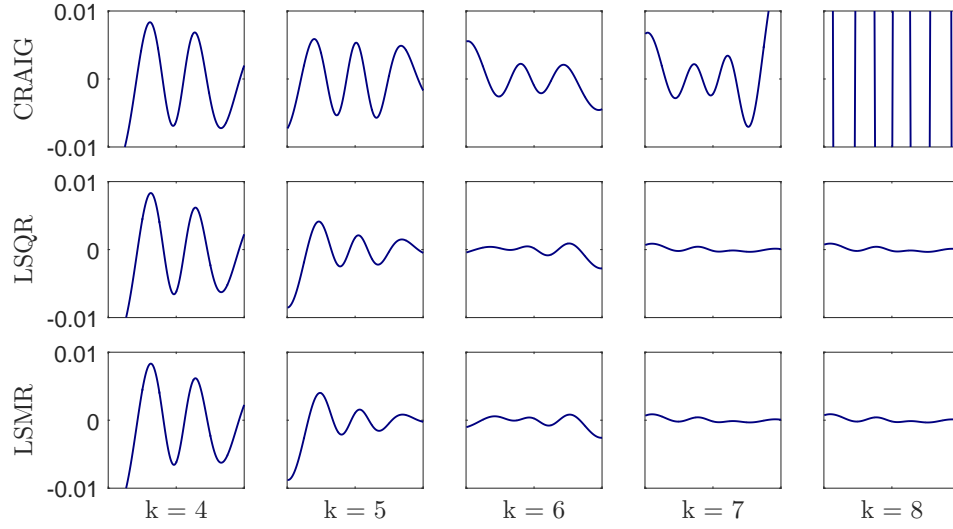
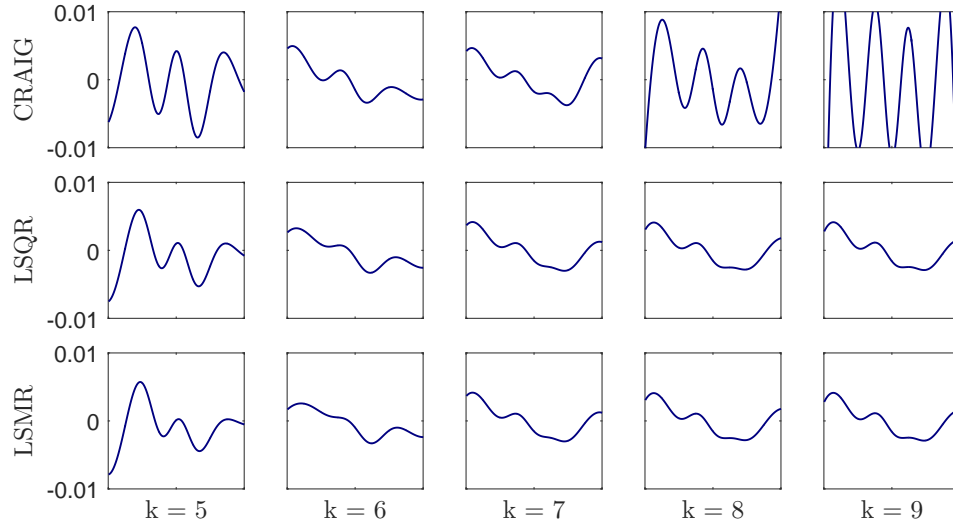


Figure 9: The size of the error of LSMR and LSQR in comparison with the inverse of the size of $\psi_k(0)$ for various test problems with various noise characteristics. Since $|\psi_k(0)|$ often grow on average till very late iterations, the semiconvergence curves exhibit similar behavior. In Figure (f) without reorthogonalization.



(a) $\eta - r_k$, white noise



(b) $\eta - r_k$, red noise

Figure 10: Difference between the noise vector and the residual of considered iterative methods for the problem **shaw** with white and red noise noise, $\delta_{\text{noise}} = 10^{-3}$. Residuals of LSQR and LSMR have similar approximation properties with respect to the noise vector.

4 Numerical experiments for 2D problems

In this section we discuss validity of the conclusions made above for larger 2D inverse problems, where the smoothing property of A (revealing itself in the decay of singular values) is typically less significant. Consequently, noise propagation in the bidiagonalization process may be more complicated; see also [36]. However, we illustrate that essential aspects of the behavior described in previous sections are still present. Note that all experiments in this section are computed *without* reorthogonalization. We consider the following 2D benchmarks:

Medical tomography problem — a simplified 2D model of X-ray medical tomography adopted from [31], function `paralleltomo(256,0:179,362)`. The data is represented the 256-by-256 discretization of the Shepp–Logan phantom projected in angles $\theta = 0^\circ, 1^\circ, \dots, 179^\circ$ by 362 parallel rays, resulting in a linear algebraic problem with $A \in \mathbb{R}^{65160 \times 65536}$. We use Poisson-type additive noise η generated as follows (see [34, chap. 2.6] and [35]) to simulate physically realistic noise:

```
A = paralleltomo(N,theta)/N; % forward model
t = exp(-A*x);               % transmission probabilities
c = poissrnd(t*N0);           % photon counts
eta = -log(c/N0);             % noisy measurements
```

where $N_0 = 10^5$ denotes the mean number of photons, resulting in the noise level $\delta_{\text{noise}} \approx 0.028$. We refer to this test problem as `paralleltomo`.

Seismic tomography problem — a simplified 2D model of seismic tomography adopted from [31], function `seismictomo(100,100,200)`. The data is represented by a 100-by-100 discretization of a vertical domain intersecting two tectonic plates with 100 sources located on its right boundary and 200 receivers (seismographs), resulting in a linear algebraic problem with $A \in \mathbb{R}^{20000 \times 10000}$. The right-hand side is polluted with additive white noise with $\delta_{\text{noise}} = 0.01$. We refer to this test problem as `seismictomo`.

Image deblurring problem — an image deblurring problem with spatially variant blur adopted from [32, 33], data `VariantGaussianBlur1`. The data is represented by a monochrome microscopic 316-by-316 image of a grain blurred by spatially variant Gaussian blur (with 49 different point-spread functions), resulting in a linear algebraic problem with $A \in \mathbb{R}^{99856 \times 99856}$. The right-hand side is polluted with additive white noise with $\delta_{\text{noise}} = 0.01$. We refer to this test problem as `vargaussianblur`.

Figure 11 shows the absolute terms of the Lanczos polynomials φ_k and ψ_k . We can identify the two phases of the behavior of $\varphi_k(0)$ – average growth and average decay. However, the transition does not take place in one particular (noise revealing) iteration, but rather in a few subsequent steps, which we refer to as the *noise revealing phase* of the bidiagonalization process. The size of $\psi_k(0)$ grows on average till late iterations, however, we often observe here that the speed of this growth slows down after the noise revealing phase. In conclusion, both curves $|\varphi_k(0)|$ and $|\psi_k(0)|$ can be flatter than for 1D problem considered in previous sections. This can be further pronounced for problems with low noise levels.

Figure 12 shows several (appropriately reshaped) left bidiagonalization vectors s_k and their cumulative periodograms for the problem `seismictomo`. Even though it is hard to make clear conclusions based on the vectors s_k themselves, we see that the periodogram for $k = 10$ is flatter than the periodograms for smaller or larger values of k , meaning that s_{10} resembles most white noise. This corresponds to Figure 11b showing that s_{10} belongs to the noise revealing phase of the bidiagonalization process. Note that similar flatter periodograms can be obtained for other few vectors belonging to this phase.

The absence of one particular noise revealing vector makes the direct comparison between s_k and the exact noise vector η irrelevant here. However, Propositions 1–3 remain valid and the overall behavior of the terms $|\varphi_k(0)|$ and $|\psi_k(0)|$ is as expected, allowing comparing the bidiagonalization-based methods. Figure 13 gives comparisons of CRAIG, LSQR and LSMR for all considered 2D test problems, analogous to Figure 6,

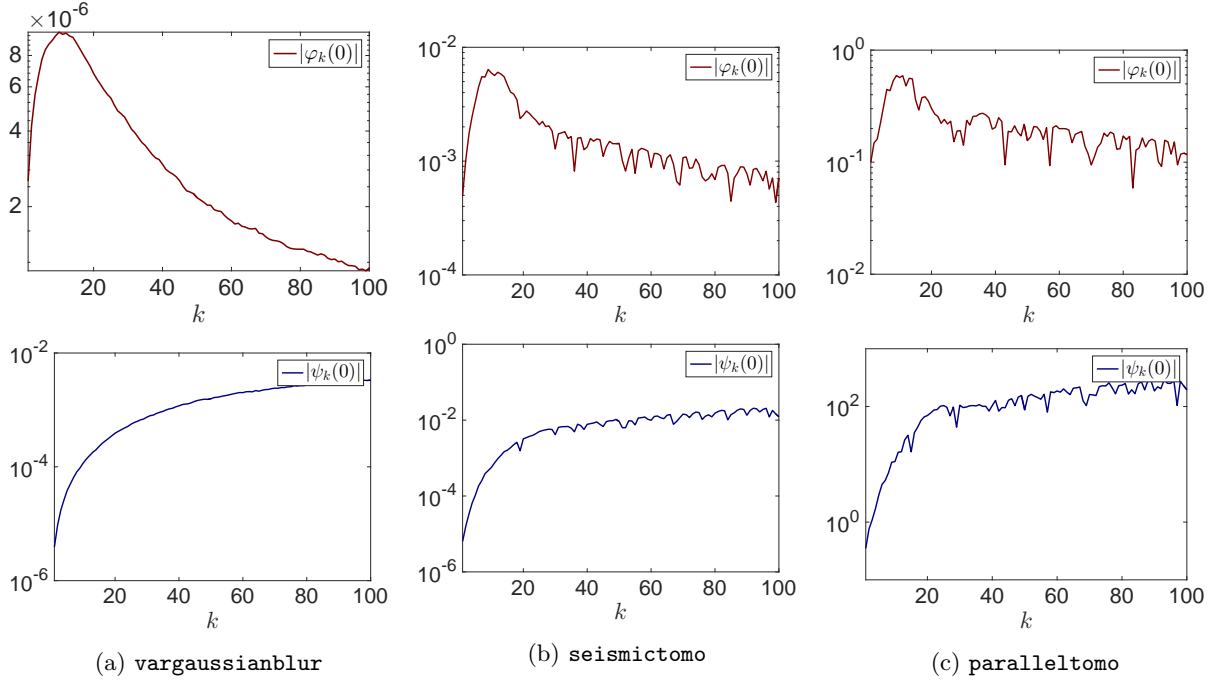


Figure 11: The size of the absolute term of the Lanczos polynomials φ_k and ψ_k for selected 2D problems contaminated by noise as described in the text. For all problems $\delta_{\text{noise}} \approx 10^{-2}$. Computed without reorthogonalization.

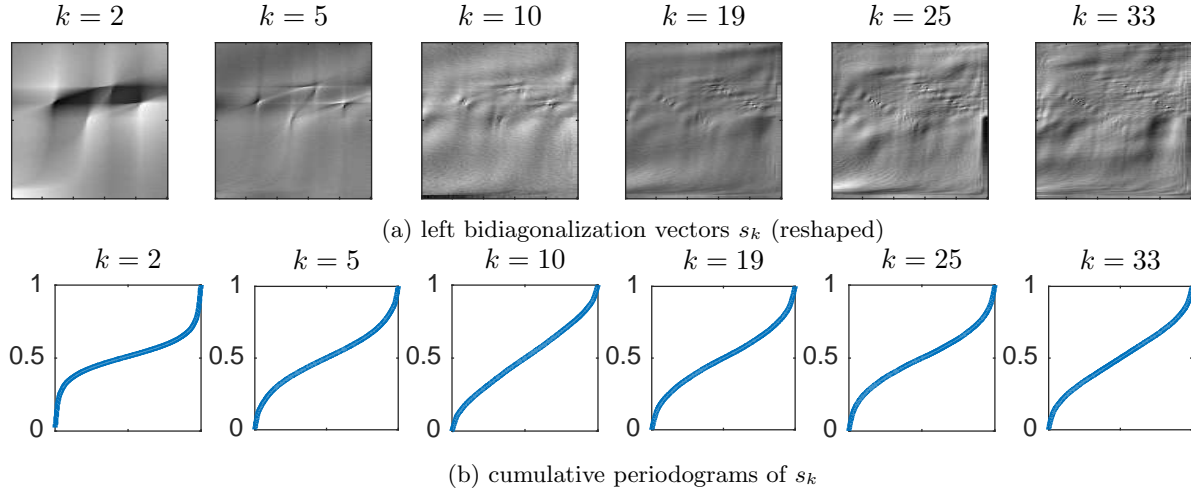


Figure 12: Left bidiagonalization vectors s_k for the problem **seismictomo** and their cumulative periodograms. The periodogram of the vector s_{10} belonging to the noise revealing phase of the bidiagonalization process is flatter. Computed without reorthogonalization.

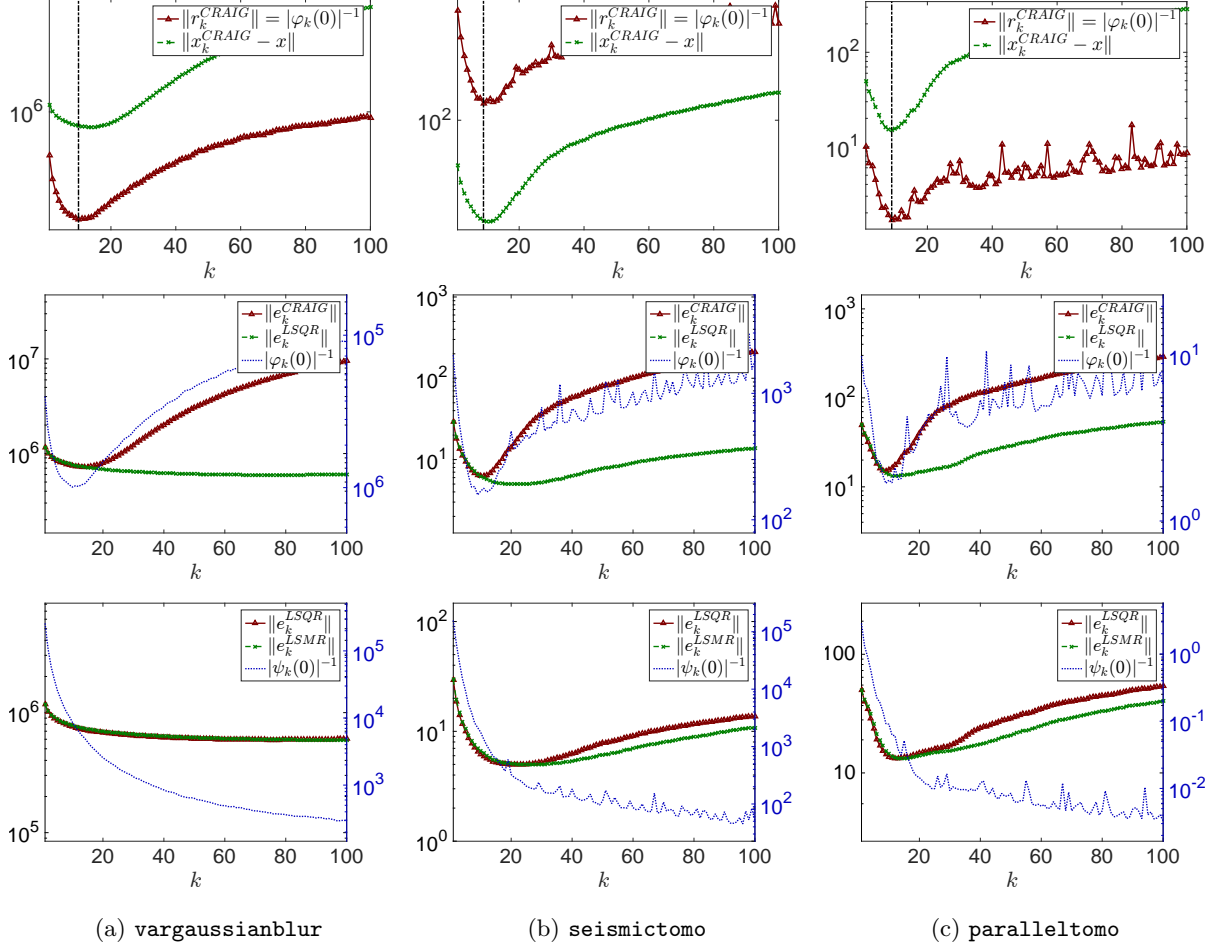


Figure 13: First row: The size of the residual and the size of the error in CRAIG. Vertical line illustrates the minimum. Second row: The size of the error of CRAIG and LSQR, together with the rescaled inverse of the amplification factor $\varphi_k(0)$ (vertical scale on the right). Third row: The size of the error of LSQR and CRAIG, together with the rescaled inverse of the factor $\psi_k(0)$ (vertical scale on the right). Computed without reorthogonalization.

7, and 9. The first row of Figure 13 shows that the CRAIG error is minimized approximately in the noise revealing phase, i.e., when the residual is minimal, see Section 3.1. The minimum is emphasized by the vertical line.

The second row of Figure 13 compares the errors of CRAIG and LSQR. According to the derivations in Section 3.2, the curves are similar before the noise revealing phase, after which they separate with CRAIG diverging more quickly. Note that the size of the inverted amplification factor $\varphi_k(0)$ is included to illustrate the noise revealing phase and has different scaling (specified on the right).

The third row of Figure 13 shows the errors of LSQR and LSMR with the underlying size of the inverted factor $\psi_k(0)$ (scaling specified on the right). The errors behave similarly as long as $|\psi_k(0)|^{-1}$ decays rapidly, see Section 3.3. The LSMR solution is slightly less sensitive to the particular choice of the number of bidiagonalization iterations k , which is a well know property [9].

5 Conclusion

We proved that approximating the solution of an inverse problem by the k th iterate of CRAIG is mathematically equivalent to solving consistent linear algebraic problem with the same matrix and a right-hand side, where a particular (typically high-frequency) part of noise is removed. Using the analysis of noise propagation, we showed that the size of the CRAIG residual is given by the inverted noise amplification factor, which explains why optimal regularization properties are often obtained when the minimal residual is reached. For LSQR and LSMR, the residual is a linear combination of the left bidiagonalization vectors. The representation of these vectors in the residuals is determined by the amplification factor, in particular, left bidiagonalization vectors with larger amount of propagated noise are on average represented with a larger coefficient in both methods. These results were used in 1D problems to compare the methods in terms of matching between the residuals and the unknown noise vector. For large 2D (or 3D) problems the direct comparison of the vectors may not be possible, since noise reveals itself in a few subsequent bidiagonalization vectors (noise revealing phase of bidiagonalization) instead of in one particular iteration. However, the conclusions on the methods themselves remain generally valid. Presented results contribute to understanding of the behavior of the methods when solving noise-contaminated inverse problems.

Acknowledgment

Research supported in part by the Grant Agency of the Czech Republic under the grant 17-04150J. Work of the first and the second author supported in part by Charles University, project GAUK 196216. The authors are grateful to the anonymous referee for useful suggestions and comments that improved the presentation of the paper.

References

References

- [1] P. Hansen, Discrete inverse problems, Society for Industrial and Applied Mathematics, 2010. arXiv:<http://epubs.siam.org/doi/pdf/10.1137/1.9780898718836>, doi:10.1137/1.9780898718836. URL <http://epubs.siam.org/doi/abs/10.1137/1.9780898718836>
- [2] P. Hansen, Rank-deficient and discrete ill-posed problems, Society for Industrial and Applied Mathematics, 1998. arXiv:<http://epubs.siam.org/doi/pdf/10.1137/1.9780898719697>, doi:10.1137/1.9780898719697. URL <http://epubs.siam.org/doi/abs/10.1137/1.9780898719697>
- [3] C. C. Paige, M. A. Saunders, LSQR: an algorithm for sparse linear equations and sparse least squares, ACM Trans. Math. Software 8 (1) (1982) 43–71. doi:10.1145/355984.355989. URL <http://dx.doi.org/10.1145/355984.355989>
- [4] Å. Björck, A bidiagonalization algorithm for solving large and sparse ill-posed systems of linear equations, BIT 28 (3) (1988) 659–670. doi:10.1007/BF01941141. URL <http://dx.doi.org/10.1007/BF01941141>
- [5] M. A. Saunders, Computing projections with LSQR, BIT 37 (1) (1997) 96–104. doi:10.1007/BF02510175. URL <http://dx.doi.org/10.1007/BF02510175>
- [6] T. K. Jensen, P. C. Hansen, Iterative regularization with minimum-residual methods, BIT 47 (1) (2007) 103–120. doi:10.1007/s10543-006-0109-5. URL <http://dx.doi.org/10.1007/s10543-006-0109-5>

- [7] E. J. Craig, The N -step iteration procedures, *J. Math. Phys.* 34 (1955) 64–73.
- [8] M. A. Saunders, Solution of sparse rectangular systems using LSQR and Craig, *BIT* 35 (4) (1995) 588–604. doi:10.1007/BF01739829.
URL <http://dx.doi.org/10.1007/BF01739829>
- [9] D. C.-L. Fong, M. Saunders, LSMR: an iterative algorithm for sparse least-squares problems, *SIAM J. Sci. Comput.* 33 (5) (2011) 2950–2971. doi:10.1137/10079687X.
URL <http://dx.doi.org/10.1137/10079687X>
- [10] M. Arioli, D. Orban, Iterative methods for symmetric quasi-definite linear systems—Part I: Theory (2013).
- [11] K. Morikuni, K. Hayami, Inner-iteration Krylov subspace methods for least squares problems, *SIAM J. Matrix Anal. Appl.* 34 (1) (2013) 1–22. doi:10.1137/110828472.
URL <http://dx.doi.org/10.1137/110828472>
- [12] G. Golub, W. Kahan, Calculating the singular values and pseudo-inverse of a matrix, *SIAM: Series B, Numerical Analysis* 2 (1965) 205–224.
- [13] M. Hanke, On Lanczos based methods for the regularization of discrete ill-posed problems, *BIT* 41 (5, suppl.) (2001) 1008–1018, *BIT 40th Anniversary Meeting*. doi:10.1023/A:1021941328858.
URL <http://dx.doi.org/10.1023/A:1021941328858>
- [14] M. E. Kilmer, D. P. O’Leary, Choosing regularization parameters in iterative methods for ill-posed problems, *SIAM J. Matrix Anal. Appl.* 22 (4) (2001) 1204–1221. doi:10.1137/S0895479899345960.
URL <http://dx.doi.org/10.1137/S0895479899345960>
- [15] J. Chung, K. Palmer, A hybrid LSMR algorithm for large-scale Tikhonov regularization, *SIAM J. Sci. Comput.* 37 (5) (2015) 562–580. doi:10.1137/140975024.
URL <http://dx.doi.org/10.1137/140975024>
- [16] V. A. Morozov, On the solution of functional equations by the method of regularization, *Soviet mathematics – Doklady* 7 (1966) 414–417.
- [17] B. W. Rust, Parameter selection for constrained solutions to ill-posed problems, *Computing science and statistics* 32 (2000) 333–347.
- [18] B. W. Rust, D. P. O’Leary, Residual periodograms for choosing regularization parameters for ill-posed problems, *Inverse Prob.* 24 (3) (2008) 034005. doi:10.1088/0266-5611/24/3/034005.
URL <http://dx.doi.org/10.1088/0266-5611/24/3/034005>
- [19] P. C. Hansen, M. E. Kilmer, R. H. Kjeldsen, Exploiting residual information in the parameter choice for discrete ill-posed problems, *BIT* 46 (1) (2006) 41–59. doi:10.1007/s10543-006-0042-7.
URL <http://dx.doi.org/10.1007/s10543-006-0042-7>
- [20] I. Hnětýnková, M. Plešinger, Z. Strakoš, The regularizing effect of the Golub-Kahan iterative bidiagonalization and revealing the noise level in the data, *BIT* 49 (4) (2009) 669–696. doi:10.1007/s10543-009-0239-7.
URL <http://dx.doi.org/10.1007/s10543-009-0239-7>
- [21] Y. Saad, Iterative methods for sparse linear systems, 2nd Edition, Society for Industrial and Applied Mathematics, Philadelphia, PA, 2003. doi:10.1137/1.9780898718003.
URL <http://dx.doi.org/10.1137/1.9780898718003>
- [22] P. C. Hansen, Regularization Tools version 4.0 for Matlab 7.3, *Numerical Algorithms* 46 (2) (2007) 189–194. doi:10.1007/s11075-007-9136-9.
URL <http://dx.doi.org/10.1007/s11075-007-9136-9>

- [23] G. Meurant, Z. Strakoš, The Lanczos and conjugate gradient algorithms in finite precision arithmetic, *Acta Numerica* 15 (2006) 471–542. doi:10.1017/S096249290626001X.
URL <http://dx.doi.org/10.1017/S096249290626001X>
- [24] G. Meurant, The Lanczos and conjugate gradient algorithms, Society for Industrial and Applied Mathematics, 2006. arXiv:<http://epubs.siam.org/doi/pdf/10.1137/1.9780898718140>, doi:10.1137/1.9780898718140.
URL <http://epubs.siam.org/doi/abs/10.1137/1.9780898718140>
- [25] G. H. Golub, G. Meurant, *Matrices, moments and quadrature with applications*, Princeton University Press, 2009.
- [26] P. C. Hansen, Regularization tools: a Matlab package for analysis and solution of discrete ill-posed problems, *Numerical Algorithms* 6 (1-2) (1994) 1–35. doi:10.1007/BF02149761.
URL <http://dx.doi.org/10.1007/BF02149761>
- [27] R. G. Brown, P. Y. Hwang, *Introduction to random signals and applied kalman filtering: with matlab exercises and solutions*, *Introduction to random signals and applied Kalman filtering: with MATLAB exercises and solutions*, by Brown, Robert Grover.; Hwang, Patrick YC New York: Wiley, c1997.
- [28] T. Gergelits, *Analysis of Krylov subspace methods*, Master’s thesis, Charles University in Prague (2013).
- [29] J. Cullum, A. Greenbaum, Relations between Galerkin and norm-minimizing iterative methods for solving linear systems, *SIAM J. Matrix Anal. Appl.* 17 (2) (1996) 223–247. doi:10.1137/S0895479893246765.
URL <http://dx.doi.org/10.1137/S0895479893246765>
- [30] M. Michenková, *Regularization techniques based on the least squares method*, Master’s thesis, Charles University in Prague (2013).
- [31] P. C. Hansen, M. Saxild-Hansen, AIR-tools—a MATLAB package of algebraic iterative reconstruction methods, *J. Comput. Appl. Math.* 236 (8) (2012) 2167–2178. doi:10.1016/j.cam.2011.09.039.
URL <http://dx.doi.org/10.1016/j.cam.2011.09.039>
- [32] S. Berisha, J. G. Nagy, *Iterative methods for image restoration*, Vol. 4, Academic Press Library in Signal Processing, 2013, Ch. 7, pp. 193–247. doi:10.1016/b978-0-12-396501-1.00007-8.
- [33] J. G. Nagy, K. Palmer, L. Perrone, Iterative methods for image deblurring: a Matlab object-oriented approach, *Numerical Algorithms* 36 (1) (2004) 73–93. doi:10.1023/B:NUMA.0000027762.08431.64.
URL <http://dx.doi.org/10.1023/B:NUMA.0000027762.08431.64>
- [34] T. Buzug, *Computed Tomography: From Photon Statistics to Modern Cone-Beam CT*. Springer-Verlag, Berlin, Heidelberg, 2008.
- [35] M. S. Andersen, J. S. Jørgensen, *Statistical models in X-ray computed tomography*. Unpublished manuscript (February 13, 2014), DTU Compute, Technical University of Denmark.
- [36] I. Hnětynková, M. Kubínová, M. Plešinger, Notes on performance of bidiagonalization-based estimator in image deblurring, *Proceedings of Algoritmy 2016 - 20th Conference on Scientific Computing*, Publishing House of Slovak University of Technology (2016), 333–342.